WAVELETS FOR CAMERA SELF-CALIBRATION AND ITS DEVELOPMENT IN NCKU

Jaan-Rong Tsay[1] and Jun-Fu Ye[2]

[1]Associate Professor, Department of Geomatics, National Cheng Kung University(NCKU)

No. 1, University Road, East Dist., Tainan City 701401, Taiwan
Email: tsayjr@mail.ncku.edu.tw

[2]Graduate Student, Department of Geomatics, NCKU
No. 1, University Road, East Dist., Tainan City 701401, Taiwan
Email: junfu.ye@gmail.com

KEY WORDS: wavelets, digital camera, self-calibration, bundle block adjustment, photogrammetry

ABSTRACT: The technical design and development of wavelets for self-calibrating diverse kinds of modern digital cameras since 2015 in NCKU, Taiwan, is reviewed briefly. Many tests are done by using some test data sets both in Taiwan and Germany. Test results are evaluated using high-precision ground checkpoints and the statistic indices. The computation software system was developed by Mr. Jun-Fu Ye in NCKU, Taiwan. Test results demonstrate the success and applicability of this new method based on orthonormal wavelets for the self-calibration of different digital cameras such as aerial digital mapping cameras, non-metric cameras on UAV, industrial cameras on MMS.

1. INTRODUCTION

1.1 Motivation and Aims

Diverse kinds of digital cameras continue to be developed so that camera calibration becomes a vital subject in photogrammetry, computer vision, and optical engineering for the purpose of calibrating the lens distortion of cameras. Therefore, additional parameters have often been used since the 1970s in the self-calibrated bundle block adjustment. Also, physical and mathematical additional parameters were proposed for analog single-head camera calibration. However, these additional parameters might not be suitable for each kind of digital camera system, such as push-broom, multi-head, virtual image composition, various image formats, fisheye camera, and so on. In addition, many additional parameters might be highly correlated with other parameters such as interior and exterior orientation parameters. A new model of Fourier additional parameters has been thus developed in recent years in Stuttgart, Germany. Fourier additional parameters are orthogonal, mathematically rigorous, flexible, generic, and efficient for camera self-calibration. The kernel functions in Fourier theory are sine and cosine functions, which are typical stationary signals. However, the lens distortion signal might be not stationary for some modern cameras. Wavelets are not only able to describe and analyze nonstationary signals, but also own the same advantages as Fourier additional parameters. Hence, a new model for camera self-calibration has been developed based on orthonormal wavelets in the past seven years in NCKU, Taiwan. This new model is expected to be able to improve the quality of photogrammetric products by utilizing cheaper cameras.

1.2 Paper Review

So far, diverse camera calibration methods have been used in photogrammetry, including laboratory calibration, test field calibration, plumb-line calibration, in-situ calibration, and self-calibration (Clarke and Fryer, 1998). Among them, self-calibration is the most flexible because it can select the "vital and significant" additional parameters (APs) automatically. APs were first developed based on mathematics or physical phenomena. For instance, Brown (1971) used physical additional parameters for close-range camera calibration and then extended for aerial camera (Brown, 1976). El-Hakim & Faig(1977) applied spherical harmonics. Ebner (1976) and Grün (1978) utilized the second and the fourth-order algebraic polynomial APs, respectively. Nevertheless, improper APs might cause problems of over-parameterization and high correlation (Clarke and Fryer, 1998). Over-parameterization might lead to a singular or ill-conditioned normal equation system. Nevertheless, these traditional self-calibration models are also continuously used in the era of digital photogrammetry to calibrate different kinds of modern digital aerial cameras although they might not be suitable for accurately calibrating the lens distortion (Fritsch, 2015). Cramer (2009) and Jacobsen et al. (2010) calibrated a variety of digital aerial cameras with different self-calibration models to correct the lens distortion of these cameras and verify their results. However, some of the aforementioned inherent defects of traditional APs still exist. Therefore, Tang et al. (2012) proposed a series of Legendre self-calibration APs based on orthogonal univariate Legendre polynomials to calibrate the lens distortion of digital aerial frame cameras. The correlations of Legendre self-calibration APs are lower than those of the traditional self-calibration APs, but an inherent defect of all polynomial APs, which is not completely independent between the x and y components of camera lens distortion, still exists. Thus, Tang (2013) proposed Fourier APs which

are orthogonal, mathematically rigorous, flexible, generic, and efficient for self-calibration. However, the lens distortion signal might be nonstationary for some modern cameras. Wavelet cannot only analyze and represent nonstationary signals, but also has the same advantages as Fourier APs. Hence, we have developed a new model called wavelet APs(WAPs).

2. WAVELETS FOR SIGNAL REPRESENTATION

Wavelet theory and wavelet functions provide the second-generation tool for signal and image processing, whereas the well-known Fourier theory and its kernel functions, namely sinusoidal and cosine functions in different frequency bands, give the first-generation tool for signal and image processing. They include the wavelet series, continuous wavelet transform (CWT), discrete wavelet transform (DWT), fast wavelet transform (FWT) in the wavelet tools, as well as the Fourier series, continuous Fourier transform (CFT), discrete Fourier transform (DFT), fast Fourier transform (FFT) in the Fourier tools, respectively. Wavelets are suited for the representation and processing of both nonstationary and stationary signals, while the Fourier tools are good *only* for stationary signals. If you look at a stationary signal for a few moments and then wait an hour and look at it again, it would look essentially the same, i.e. its overall level would be about the same and its amplitude distribution and standard deviation would be also about the same. In other words, signals whose frequency contents do not change over time are called *stationary signals*. In this case, one does not need to know at what time durations frequency components exist, since all frequency components exist at all time locations. The sine and cosine functions are two typical examples of stationary signal functions. Contrary to the aforementioned examples of stationary signals, those signals, whose frequency constantly changes over time, are known as non-stationary ones. For instance, the "chirp" signal is non-stationary.

Mallat (1989) proposed a theory for multiresolution signal decomposition. Multi-resolution analysis (MRA) plays an important role in the wavelet theory and is often called multiscale analysis (MSA), too. It enables an efficient decomposition and reconstruction of signals, including images, in different levels of detail. The wavelet representation can be used to display signals inclusive of two-dimensional image distortion functions.

So far, there are already diverse kinds of digital cameras such as digital frame cameras, virtual image composition cameras, multi-head cameras, fish-eye cameras, push-broom cameras, linear array cameras, and so on. They may be metric or non-metric. The inherent image distortion may be stationary or non-stationary. Wavelets can represent both stationary and non-stationary image distortion signals. Moreover, some wavelets such as Daubechies wavelet functions display a fractal geometry, even though they are continuous for the order N>1 (Kaiser, 1994). The fractal geometry is apparently the correct mathematics for describing image texture (Jaehne, 1991) and real signals in nature. Real signals in nature are often fractal or Hölder-continuous (also called "lipschitz continuous") (Daubechies, 1994; Kaiser, 1994; Louis et al., 1994). They often cannot be described by traditional analytical functions or, briefly to say, expressed in a closed form. These signals in nature often have varied degrees of continuity from place to place. On the other hand, many signals in nature are fractal and have the properties of, e.g., self-similarity or self-affinity. Due to the aforementioned considerations, wavelets are selected and applied in this study to design a new model called wavelet additional parameter (WAP), which is expected to be able to self-calibrate diverse kinds of digital cameras. Tsay (2016) proposed some original ideas for designing the WAP models, and mentioned that not only the theoretical and practical wavelet series (Strang & Nguyen, 1996) but also both the S-D model for interpolation and S-model for approximation proposed by Tsay (1996) can be extended and utilized for designing the WAP models. In this study, one of those novel models for WAP is designed, proposed, and tested. The concerned computation algorithm and the corresponding program system for self-calibrated bundle block adjustment are also developed by using the program language C# on a general personal computer.

Also, there are already diverse kinds of wavelet functions which might be available for this WAP model, such as Haar wavelets, Daubechies wavelets, Littlewood-Paley wavelet, Morlet wavelet, Meyer wavelet, Battle-Lemarie wavelets. They might be biorthogonal, orthogonal, semi-orthogonal, or nonorthogonal wavelets. On the other hand, they might be compactly supported or not compactly supported. They might be real or complex wavelets. They may be continuous or discontinuous. Their function curves may be smooth or not smooth. These diverse wavelet functions may be regular or irregular. Their function curves might be symmetric or asymmetric. Some of them can be displayed explicitly, but the others cannot be described in a closed-form expression. Anyway, the accuracy, rigorousness, and flexibility of this approximation model for image distortion and the computation complexity, namely the number of addition and multiplication operations, are taken into account in this study for selecting proper wavelet families for our WAP model. Finally, the orthonormal(=orthogonal and normalized) wavelet basis functions including asymmetric Daubechies wavelets of 4th order, least asymmetric Daubechies wavelets of 4th order, Battle-Lemarie wavelets of 4th order, and Meyer wavelets are adopted in this study for establishing the WAP model.

3. WAVELETS FOR ADDITIONAL PARAMETERS

Camera self-calibration can be regarded as a mathematical issue of function approximation. The WAP models can be incorporated into the well-known collinearity equations in photogrammetry (Wolf et al., 2014), as shown in (1a) and (1b).

$$x = x_0 - f \left[\frac{m_{11}(X-X_0)+m_{12}(Y-Y_0)+m_{13}(Z-Z_0)}{m_{31}(X-X_0)+m_{32}(Y-Y_0)+m_{33}(Z-Z_0)} \right] + \Delta x + \varepsilon_x \qquad (1a)$$

$$y = y_0 - f \left[\frac{m_{21}(X-X_0)+m_{22}(Y-Y_0)+m_{23}(Z-Z_0)}{m_{31}(X-X_0)+m_{32}(Y-Y_0)+m_{33}(Z-Z_0)} \right] + \Delta y + \varepsilon_y \qquad (1b)$$

where x and y are photo coordinates of an image point of interest; X, Y, and Z are the object coordinates of its corresponding object point; f is the camera focal length; x_0 and y_0 are the photo coordinates of the principal point; X_0, Y_0, and Z_0 are the object coordinates of camera exposure station; m's are the functions of three rotation angles, e.g. omega ω, phi ϕ, and kappa κ; Δx and Δy are the systematic error components in the photo coordinates x and y, respectively; ε_x and ε_y are the random error components in the photo coordinate observations x and y, respectively. The systematic error components Δx and Δy in (1a) and (1b) can be defined as (2a) and (2b), respectively,

$$\Delta x = \Delta x \left(x, y, W, H, s_x, s_y, \phi_N, a_{jk} \right) \qquad (2a)$$
$$\Delta y = \Delta y \left(x, y, W, H, s_x, s_y, \phi_N, b_{jk} \right) \ldots\ldots\ldots\ldots\ldots\ldots\ldots\ldots(2b)$$

where W and H are the width and height of the image, respectively; s_x and s_y are the scale factors of the wavelet basis functions in the x and y directions, respectively; a_{jk} and b_{jk} are the WAPs in Δx and Δy, respectively; j and k are the translation parameters of the wavelet basis functions in the x and y directions, respectively; ϕ is the adopted orthonormal father wavelet function of order N.

4. WAP DEVELOPMENT IN NCKU

The first version of WAP programs was developed in 2015 to 2016, and they are then extended to new versions with more and more functions in the years 2016 to 2023. For example, the Cholesky decomposition, namely the Cholesky factorization, and the Gauss elimination method are added to our computation programs. The method of dual quaternions (Daniilidis, 1999) is also then applied to determine the initial values of the exterior orientation elements of any image. The corresponding solution systems are developed for vertical photography, (high) oblique photography, close-range photography, terrestrial photography, and photography on an MMS . On the other hand, different kinds of orthonormal (=orthogonal and normalized) wavelets are added and applied. They are the family of asymmetric Daubechies wavelets, the family of least asymmetric Daubechies wavelets, the family of Battle-Lemarie wavelets, and Meyer wavelets. The automatic sorting of all unknowns in the AT as well as the automatic determination of initial values of unknowns are added to the system of programs. Also, these programs are refined year by year. Moreover, a plenty of tests are done by using diverse test data sets in Taiwan and Germany including images taken with aerial mapping cameras, nonmetric cameras on UAV and MMS. The test results are evaluated by means of independent checkpoints, e.g. in the calibration field. Moreover, some statistical tests are also applied such as correlation tests, significance tests, and total correlation. The corresponding thresholds used in BINGO(Kruck, 2015) are adopted in our tests. These test results are shown and analyzed briefly as follows.

5. TESTS AND ANALYSES

5.1 Aerial Metric Camera

The test cases use aerial images taken with an aerial metric camera UltraCam XP to perform bundle block adjustments without or with WAPs, where the signalized points with both the horizontal and vertical accuracy of less than 1cm are used as GCPs and CHKs in the calibration field. Also, asymmetric Daubechies wavelets of the 3rd order are used in these tests. As shown in Figure 3 and Table 3, test results demonstrate that the $\hat{\sigma}_0$-value is reduced and the RMS values of ground coordinate differences on all checkpoints are improved after WAPs are used in the three kinds of image coverage as mentioned in Table 2. For the two cases 1-2 and 2-2 with WAPs, the external accuracy is about 0.48 to 0.54 GSD in the horizontal direction, and about 0.70 to 0.85 GSD in the vertical direction, respectively. For the case 3-2 with WAPs, the external accuracy is about 0.28 GSD and about 0.43 GSD in the horizontal and vertical directions, respectively. These test results demonstrate that this wavelet model for self-calibrated bundle block adjustment is helpful and applicable to correct the systematic distortion errors of images taken with aerial digital mapping cameras.

Table 1. The parameters of the test images taken with the aerial metric camera UltraCam XP

Acquisition date	21 September 2012		Side lap %	≈ 60
Camera	UltraCam XP wide angle		Flight height (AGL)	≈ 545m
Focal length	70.500±0.002mm		Groundel size	≈ 46mm
Pixel size	6.0μm		Image scale	$\approx 1:7700$
Image size	11310 x 17310 pixels		Calibration field size	750m x 600m
End lap %	≈ 80		Ground coverage	≈ 1433m x 1433m

Table 2. Test cases 1-1 ~ 3-2

	Without WAP	With WAPs
North-south flight strips (9 GCPs, 42 CHKs)	Case 1-1	Case 1-2
East-west flight strips (9 GCPs, 41 CHKs)	Case 2-1	Case 2-2
Cross flight strips (9 GCPs, 49 CHKs)	Case 3-1	Case 3-2

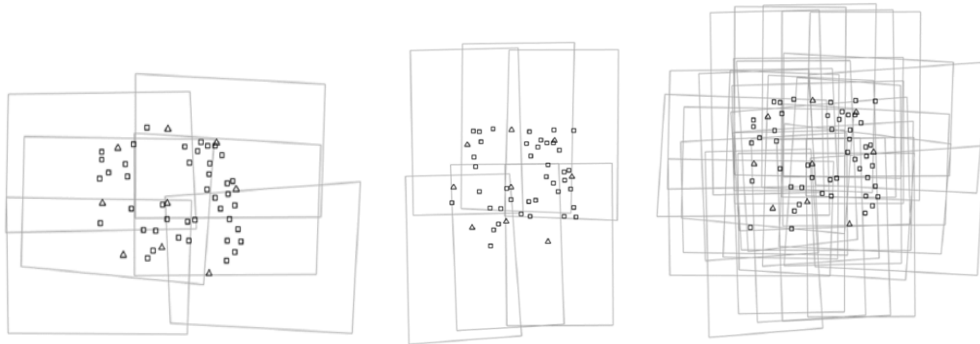Figure 1. Location of the test area in Taiwan and its image coverage

Figure 2. The distribution maps of all used known points, where Δ and □ denote the full GCPs and the full CHKs, respectively, and the image overlap of all used images in Case 1 (left), Case 2 (middle), and Case 3 (right)

Table 3. The computation parameters and test results in all cases of the aerial metric camera UltraCam XP

Case	Scale factor: s_x, s_y	Number of WAPs	$\hat{\sigma}_0(\mu m)$	Degree of freedom	Average redundancy	Computation time
1-1	-	-	1.98	1401	0.36	<1s
1-2	0.65, 0.63	49/234	1.64	1325	0.34	3s
2-1	-	-	1.67	1368	0.33	<1s
2-2	0.65, 0.63	48/234	1.34	1286	0.32	4s
3-1	-	-	2.24	22644	0.80	15s
3-2	0.65, 0.63	108/234	1.64	21914	0.79	93s
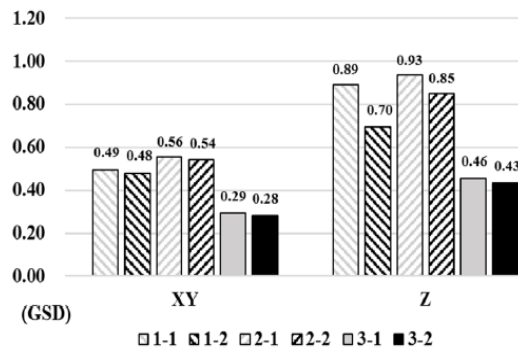
Figure 3. The RMS value of ground coordinate differences on all checkpoints (1GSD≈4.6cm)

Another set of tests using aerial images taken with an aerial digital mapping camera DMC in the Vaihingen/Enz test field near Stuttgart, Germany, was done, too. The signalized points with horizontal and vertical accuracy of about 1cm and 2cm, respectively, (Cramer, 2010) are used as GCPs and CHKs. As shown in Figure 6 and Table 6, where the

asymmetric Daubechies wavelets of the 3rd order are used in the test cases B and D, test results demonstrate again that the $\hat{\sigma}_0$-value is reduced and the RMS values of ground coordinate differences on all checkpoints are decreased after WAPs are used in the four cases A~D as mentioned in Table 5. For example, the RMS values of ground elevation differences (dZs) on all checkpoints are reduced from 1.34GSD to 0.43GSD and from 0.89GSD to 0.43GSD for the aerial triangulation without or with GNSS/IMU observations for the exterior orientation elements of all images, respectively, after WAPs are used.

Figure 4. The Vaihingen/Enz test field near Stuttgart, Germany (Tang, 2013)
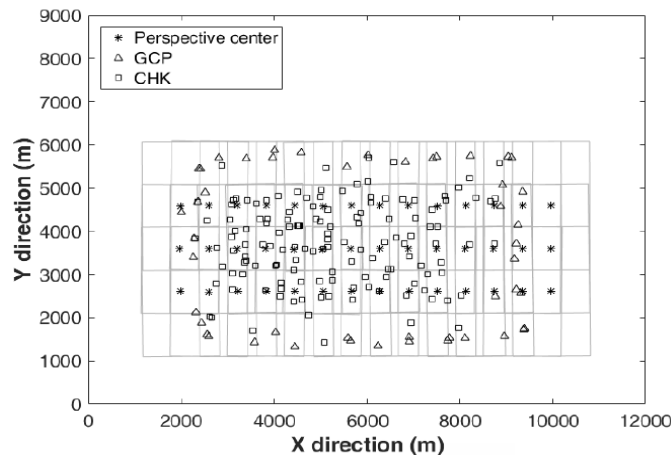
Figure 5. The distribution maps of all used known points, where Δ, □, and * denote the full GCPs, the full CHKs, and the perspective centers, respectively, and the overlap of all used images

Table 4. The parameters of the test images taken with the aerial digital mapping camera DMC

Camera	DMC		Side lap %	60 ~ 70
Focal length	120.000 mm		Flight height (AGL)	$\approx$ 2170 m
Pixel size	12.0μm		Groundel size	$\approx$ 21.6 cm
Image size	7680 x 13824 pixels		Image scale	$\approx$ 1:18000
End lap %	60 ~ 70		Ground coverage	$\approx$ 10km x 5km

Table 5. Test cases A ~ D

Case	Case description
A	AT without APs
B	AT with WAPs
C	GNSS/IMU supported AT without APs
D	GNSS/IMU supported AT with WAPs

Table 6. The computation parameters and test results in all cases of the digital mapping camera DMC

Case	Number of WAPs	$\hat{\sigma}_0$(pixel)	Average redundancy	Number of full GCP	Number of full CHKs
A	-	0.183	0.67	44	138
B	116/234	0.135	0.65	46	136
C	-	0.187	0.68	45	138
D	116/234	0.137	0.66	46	138
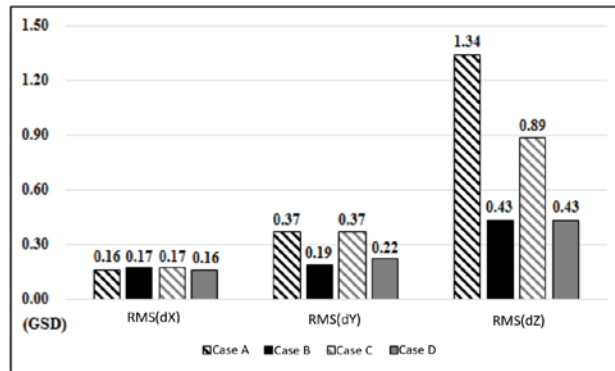
Figure 6. The RMS value of ground coordinate differences on all checkpoints (1GSD≈21.6cm)

5.2 Non-metric digital camera on UAV

Another set of images taken with the non-metric digital camera Sony A7RII on a UAV is also utilized for our tests. Their image parameters are shown in Table 7. Considering the efficiency of unmanned aircraft systems (UAS) with this small-format camera, a total of 210 aerial images provided by Strong Engineering Consulting Co., Ltd. were stored in JPEG format. Therefore, there are some challenges in measuring the image coordinates of known points. Some sample images of ground targets from metric and non-metric digital cameras, respectively, are shown in Figure 7. The same number on the picture indicates the same ground target image taken on the closest exposure station. Some sample images were selected to calculate their blur parameter values and modulation transfer function (MTF) values. As shown in Table 8, the quality of images taken with non-metric camera is apparently inferior to the metric camera. The results of the bundle block adjustment without additional parameters (Case 4-1) and by using WAPs (Case 4-2) are shown in Table 9, where the asymmetric Daubechies wavelets of the 3rd order are used in this test case 4-2. The $\hat{\sigma}_0$-value is significantly reduced from 6.9μm to 4.6μm after using WAPs. However, the vectors of horizontal and vertical coordinate differences on all checkpoints shown in Figure 8 indicate that there are still some blunders in the adjustment results. Further studies and improvements should be made.

Table 7. The parameters of the test images taken with the non-metric camera Sony A7RII on UAV

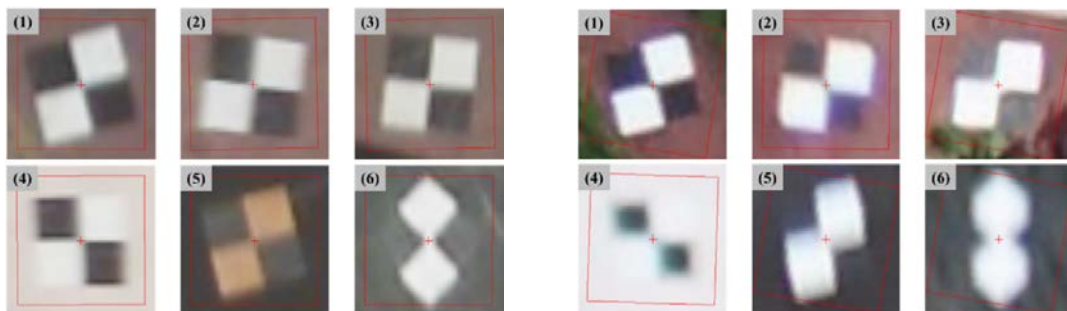| Acquisition date	14 August 2018		Side lap %	≈60
Camera	Sony A7RII		Flight height (AGL)	≈ 400 m
Focal length	35 mm		Groundel size	≈ 5.2 cm
Pixel size	4.51 μm		Image scale	≈ 1:11400
Image size	7952 x 5304 pixels		Calibration field size	750m x 600m
End lap %	≈80		Ground coverage	≈ 1000m x 1000m

Figure 7. The sample images of ground targets taken with metric(left) and non-metric (right) digital cameras

Table 8. Image quality: blur parameter and MTF of sample images taken with non-metric and metric digital cameras
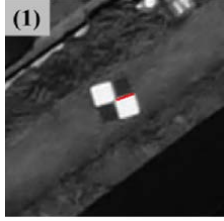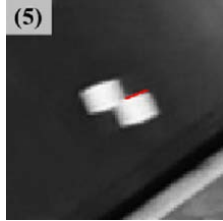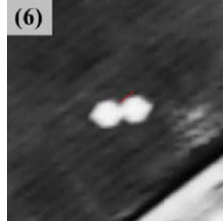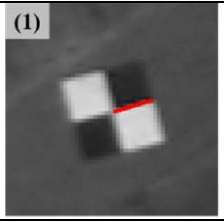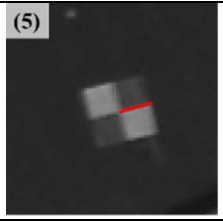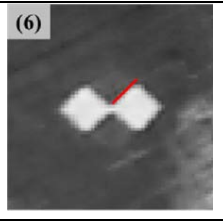
Sample images of ground targets taken with non-metric digital cameras			
Blur parameter (unit: pixel)	0.959	0.392	0.819
MTF	0.166	0.405	0.194
Sample images of ground targets taken with metric digital cameras			
Blur parameter (unit: pixel)	0.403	0.315	0.382
MTF	0.395	0.506	0.417

Table 9. The computation parameters and test results in all cases of the non-metric digital camera Sony A7RII on UAV

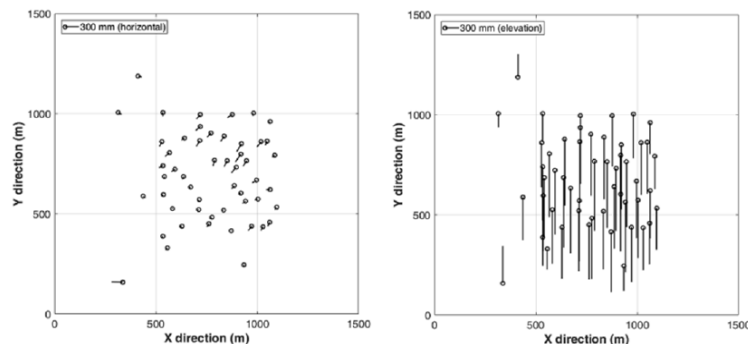| Case	Scale factor: s_x, s_y	Number of WAPs	$\hat{\sigma}_0$(μm)	Degree of freedom	Average redundancy	Computation time
4-1	-	-	6.9	52856	0.73	45 min
4-2	0.56, 0.56	153/286	4.6	50027	0.73	193 min

Figure 8. The difference vectors of horizontal coordinates (left) and elevations (right) on all checkpoints (Case 4-2)

5.3 Non-metric digital camera on MMS

Besides, tests are also done by using images provided by the National Land Surveying Center(NLSC), MOI, Taiwan, and taken with the non-metric digital camera on a mobile mapping system(MMS) in Sha-Lung, Tainan City, Taiwan. Figure 9 illustrates some sample images. This set of a huge number of MMS images is not suitable for our tests because the distribution and number of known ground points are improper and insufficient. Also, their accuracy of 3D ground coordinates is about 15cm which is not proper for our tests. Another set of MMS images is provided by the Sunrise Geomatics Co., Ltd., Taiwan, and some sample images are shown in Figure 10, which are also not applicable for our tests because there are no tie points in the sky image patches about at the middle up portion of the image frame, and the parallactic angles for those image points near the image center are close to zero. Finally, 8 available MMS images are used for our tests and are shown in Figure 11. The locations of 18 full GCPs and 13 full CHKs as well as the perspective centers of 8 MMS images are illustrated in Figure 12, where the GCPs and CHKs with the ground coordinate accuracies of $\hat{\sigma}_X$<0.7cm, $\hat{\sigma}_Y$<0.6cm, and $\hat{\sigma}_Z$<0.4cm are used. Table 10 shows the parameters of these 8 test images taken with non-metric camera Basler A102kc on MMS. The test results are shown in Table 11. The posterior standard deviation of unit weight is significantly improved, too, after using WAPs. Figure 13 illustrates the RMS values of ground coordinate differences on all checkpoints. The WAPs based on Meyer wavelets have the best performance with the RMS values 4.2cm, 6.4cm, 9.1cm of ground coordinate differences in the X, Y, and Z components, respectively. Compared with the ones without WAPs, namely 6.7cm, 8.9cm, and 12.4cm in the X, Y, and Z components, respectively, WAPs improve apparently the accuracy of the bundle block adjustment. Nevertheless, WAPs based on the least asymmetric Daubechies wavelets of 4th order (ladb4) and the Battle-Lemarie wavelets of 4th order (BL4) give worse results. They demonstrate

that there are too less images used, namely 8 images in this case, so that the results are not good. Anyway, further tests with suitable images and checkpoints should be done.

Figure 9. Sample MMS images provided by the NLSC, MOI, Taiwan

Figure 10. Sample MMS images provided by Sunrise Geomatics Co., Ltd., Taiwan

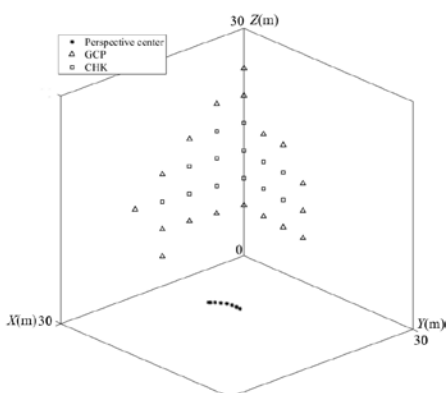Figure 11. Test images taken with the non-metric camera Basler A102kc on an MMS

Figure 12. The locations of 18 full GCPs and 13 full CHKs as well as the perspective centers of 8 MMS images

Table 10. The parameters of the test images taken with the non-metric camera Basler A102kc on an MMS

Camera	Basler A102kc		Image size	1392 x 1040 pixels
Focal length	≈ 8.2 mm		End lap %	≈ 80
Pixel size	≈ 6.45 μm			

Table 11. The computation parameters and test results in all cases of the non-metric camera Basler A102kc on an MMS

	Number of WAPs	$\hat{\sigma}_0$(pixel)	Average redundancy	Number of full GCPs	Number of full CHKs
No WAP	-	0.58	0.47	14	13
adb4	21/48	0.20	0.29	12	12
ladb4	17/40	0.20	0.29	10	12
BL4	30/48	0.18	0.33	13	12
Meyer	29/60	0.15	0.31	13	13
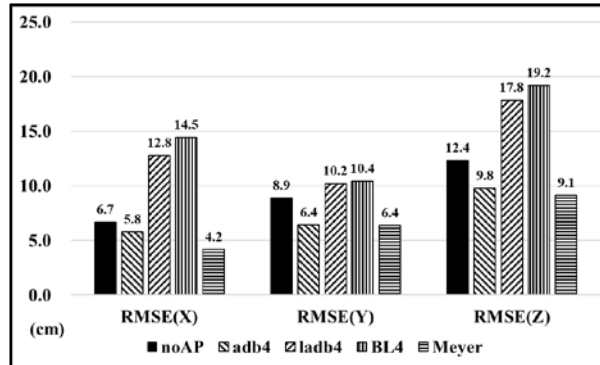
Figure 13. The RMS value of ground coordinate differences on all checkpoints

6. CONCLUDING REMARKS

The development of wavelet additional parameters (WAPs) since 2015 in NCKU is introduced concisely. Four sets of test images and ground checkpoints are used for tests. They include aerial metric camera UltraCam XP, aerial digital mapping camera DMC, non-metric digital camera Sony A7RII on a UAV, and non-metric camera Basler A102kc on MMS. These test results demonstrate that this wavelet model for self-calibrated bundle block adjustment is helpful and applicable to correct systematic distortion errors.

For example, the test cases used aerial images taken with an aerial metric camera UltraCam XP to perform bundle block adjustments without or with WAPs. As shown in Figure 3 and Table 3, test results demonstrate that the $\hat{\sigma}_0$-value is reduced and the RMS values of ground coordinate differences (RMSDs) are decreased after WAPs are used in the three kinds of image coverage as mentioned in Table 2. For the two cases 1-2 and 2-2 with WAPs, the RMSDs are about 0.48 to 0.54 GSD in the horizontal direction, and about 0.70 to 0.85 GSD in the vertical direction, respectively. For the case 3-2 with WAPs, the external accuracy is about 0.28 GSD and about 0.43 GSD in the horizontal and vertical directions, respectively.

Test results using aerial digital mapping camera DMC demonstrate that the $\hat{\sigma}_0$-value is reduced and the RMSD values on all checkpoints are decreased, too, after WAPs are used in the four cases A~D as mentioned in Table 5. For example, the RMSDs on all checkpoints are reduced from 1.34GSD to 0.43GSD and from 0.89GSD to 0.43GSD for the aerial triangulation without or with GNSS/IMU observations for the exterior orientation elements of all images, respectively, after WAPs are used.

Tests using non-metric digital camera Sony A7RII on a UAV show that the $\hat{\sigma}_0$-value is significantly reduced from 6.9μm to 4.6μm after using WAPs. However, the vectors of horizontal and vertical coordinate differences on all checkpoints shown in Figure 8 indicate that there are still some blunders in the adjustment results. Further studies and improvements should be made.

Tests using non-metric camera Basler A102kc on MMS illustrate that the WAPs based on Meyer wavelets have the best performance with the RMSD values 4.2cm, 6.4cm, 9.1cm on all checkpoints in the X, Y, and Z components, respectively. Compared with the ones without WAPs, namely 6.7cm, 8.9cm, and 12.4cm in the X, Y, and Z components, respectively, WAPs improve apparently the accuracy of the bundle block adjustment. Nevertheless, WAPs based on the least asymmetric Daubechies wavelets of 4th order (ladb4) and the Battle-Lemarie wavelets of 4th order (BL4) give worse results. They demonstrate that there are too less images used, namely 8 images in this case, so that the results are not good. Anyway, further tests with suitable images and checkpoints should be done.

7. ACKNOWLEDGEMENTS

8. REFERENCES

Brown, D., 1971. Close-range camera calibration. *Photogrammetric Engineering*, 37(8), pp.855-866.

Brown, D., 1976. The bundle method – progress and prospects. In: *International Archives of Photogrammetry*, 21 (Part 3), pp.1-33.

Clarke, T., Fryer, J., 1998. The development of camera calibration methods and models. *Photogrammetric Record*, 16(91), pp. 51-66.

Cramer, M., (Ed.), 2009. *Digital Camera Calibration*. EuroSDR official publication No. 55.

Cramer, M., 2010. *The DGPF-Test on Digital Airborne Camera Evaluation – Overview and Test Design*. PFG 02/2010, final version (status Jan 12, 2010), Stuttgart, Germany.

Daniilidis, K., 1999. Hand-eye calibration using dual quaternions. *The International Journal of Robotics Research*, 18(3), pp.286-298

Daubechies, I., 1994. *Ten Lectures on Wavelets*. Society for Industrial and Applied Mathematics, Philadelphia, PA, USA.

Ebner, H., 1976. Self-calibrating block adjustment. *Bildmessung und Luftbildwesen*, 44(4), pp.128-139.

El-Hakim, S., Faig, W., 1977. Compensation of systematic image errors using spherical harmonics. In: *Proceedings of the American Society of Photogrammetry*, Fall technical meeting, Little Rock, Arkansas, pp.492-499.

Fritsch, D., 2015. Some Stuttgart Highlights of Photogrammetry and Remote Sensing. In: *Photogrammetric Week 2015*, pp.3-20.

Grün, A., 1978. Progress in photogrammetric point determination by compensation of systematic errors and detection of gross errors. In: *International Archives of Photogrammetry*, 22 (Part 3), pp.113-140.

Jacobsen, K., Cramer, M., Ladstädter, R., Ressl, C., and Spreckels, V., 2010. DGPF-project: evaluation of digital photogrammetric camera systems – geometric performance. *Photogrammetrie-Fernerkundung-Geoinformation* (PFG), 2010(2), pp.85-98.

Jaehne, B., 1991. *Digitale Bildverarbeitung*. 2nd edition, Springer-Verlag, ISBN 3-540-53768-6.

Kaiser, G., 1994. *A Friendly Guide to Wavelets*. Birkhaeuser Boston, ISBN 0-8176-3711-7.

Kruck, Erwin J., 2015. BINGO 6.7 User's manual.

Louis, A.K., Maaβ, P., Rieder, A., 1994. *Wavelets, Theorie und Anwendungen*. B.G. Teubner Stuttgart, Germany.

Mallat, S.G., 1989. A Theory for Multiresolution Signal Decomposition: The Wavelet Representation. *IEEE Transactions on Pattern Analysis and Machine Intelligence*. 11(7), pp.674-693.

Strang, G., Nguyen, T., 1996. *Wavelets and Filter Banks*. ISBN: 0-9614088-7-1. Wellesley Cambridge Press.

Tang, R., Fritsch, D., Cramer, M., 2012. New Mathematical Self-Calibration Models in Aerial Photogrammetry. *32. Wissenschaftlich-Technische Jahrestagung der DGPF*, pp.457-469.

Tang, R., 2013. *Mathematical Methods for Camera Self Calibration in Photogrammetry and Computer Vision*. Deutsche Geodätische Kommission, Reihe C, Nr. 703, München.

Tsay, J.R., 1996. *Wavelets fuer das Facetten-Stereosehen*. Deutsche Geodaetische Kommission, Reihe C, Heft Nr. 454. Munich, Germany. ISSN 0065-5325. ISBN 3-7696-9497-X.

Tsay, J.R., 2016. *Wavelet Self-Calibrated Additional Parameters*. Research project of the Ministry of Science and Technology with the research grant MOST 105-2119-M-006-032.

Wolf, P.R., Dewitt, B.A., Wilkinson, B.E., 2014. *Elements of Photogrammetry with Applications in GIS*. 4th ed., McGraw-Hill Higher Education, pp.268-269.